# ENGINEERING Computations

Volume 4, Number 1, March 1987
ISSN 0264–4401

*Pineridge Press Limited,*
*91 West Cross Lane, West Cross,*
*Swansea, SA3 5LU, U.K.*

# Prediction of the flow, reaction and heat transfer in an oxy-fuel glass furnace*

**M. G. M. S. Carvalho, D. F. G. Durão and J. C. F. Pereira**
*Instituto Superior Tecnico, Mechanical Engineering Department, Av. Rovisco Pais, 1096 Lisbon, Codex, Portugal*
*(Received December 1986)*

## ABSTRACT

A three-dimensional computer simulation of a combustion chamber used in the glass production industry is presented. A numerical solution technique is used to solve the governing time-averaged partial differential equation and the physical modelling for turbulence, combustion and thermal radiation. A two-equation turbulence model is employed along with a combustion model based on a fast kinetics statistical approach. A radiation model is used along with the Hottel mixed grey gas model. To solve the governing differential equations an implicit technique of finite-difference kind is applied. The economy of the computations is very considerably enhanced by the separate calculation of the burner and bulk glass combustion chamber regions, in a manner which takes account of the differing physical nature of their flows. The burner outlet region is calculated with an axisymmetric model. Such two-dimensional calculations allowed a good resolution of the burner outlet, and provide the inlet conditions for the three-dimensional calculations of the glass furnace. The prediction procedure is applied to an industrial glass furnace, which operates with oxy-fuel conditions. Measurements of mean gas temperature and concentrations were performed at different locations in the furnace. The calculated flame length, temperature field and concentrations are with satisfactory agreement with the measured ones.

## INTRODUCTION

The recent awareness of the limitation of energy resources, the increase in fuel prices, and the problem of pollution have turned the combustion engineer's attention towards the importance of improving the combustion equipment design.

Increasing pressure is being placed on engineers to have recourse to every available modern theoretical and analytical means to quantify and enhance the industrial furnace performance criteria. There is currently considerable interest from the glass and ceramic industry to support the construction of a mathematical model which reliably simulates the performance of the glass melting furnaces. Glass furnaces are large and so they are extremely costly to develop by highly empirical methods.

A three-dimensional simulation of a glass furnace combustion in which the flow field and heat release were determined from a numerical solution of the governing balance equations has been presented by Gosman *et al.*[1]. The work of Carvalho and Lockwood[2] extended the aforementioned one to an industry furnace of differing configuration and brought into analysis the batch and glass tank flows.

The present work deals with the oxygen-rich atmosphere and substantial radiation present in the combustion chamber of an industrial glass furnace operating with oxy-fuel conditions. The economy of the computations was very considerably enhanced by the separate calculation of the burner and bulk glass combustion chamber region, in a manner which takes account of the differing physical nature of their flows. The burner outlet region was calculated with an axisymmetric model. Such two-dimensional calculations allowed a good resolution of the burner outlet, and provided the inlet conditions for the three-dimensional calculations of the glass furnace.

## DESCRIPTION OF THE FURNACE

*Figure 1* shows a sketch of the furnace. The fuel and oxidant are separately admitted from a single burner without swirl (1). Heavy fuel oil is admitted through a central nozzle and in the annular region of the burner the oxygen is injected through 16 holes.

The flame forms a loop within the combustion chamber and exits through the port (2). The furnace roof and side walls are refractory lined and the roof is slightly arched as indicated on the Figure. The batch enters via the port at location (3) and the molten material exits from the throat at location (4).

## PHYSICAL MODELLING

The governing transport equations for the mean motion of a turbulent three-dimensional flow were applied in their cartesian co-ordinate form.

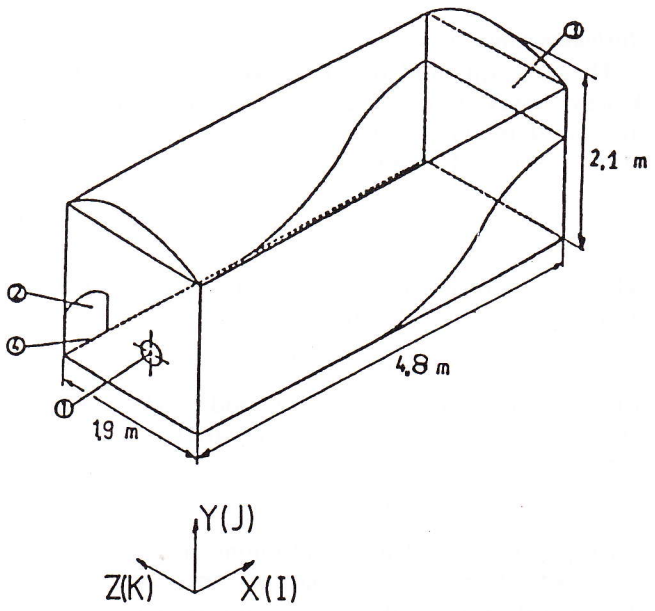


*Figure 1* Sketch of the furnace. 1, Burner; 2, outlet port; 3, feed of raw material; 4, batch outlet

* Presented at the 3rd International Conference on Numerical Methods for Non-Linear Problems, Dubrovnik, September 1986.

*Mean flow equations*

The time-averaged equations for the conservation of momentum are in compact tensor notation, as follows:

$$\frac{\partial}{\partial x_j}\left(\overline{\rho u_j}\,\overline{u_i}+\overline{p\delta_{ij}}-\mu\left[\frac{\overline{\partial u_i}}{\partial x_j}+\frac{\overline{\partial u_j}}{\partial x_i}-\frac{2}{3}\overline{\frac{\partial u_k}{\partial x_k}}\delta_{ij}\right]\right)-(\rho-\rho_{\text{ref}})g_i+\frac{\partial}{\partial x_j}\overline{\rho u_j' u_i'}=0 \quad (1)$$

Here $u_i$ is velocity in the direction of coordinate $x_i$, $\rho$ is density and $\rho_{\text{ref}}$ a reference value, $g_i$ is the magnitude of the gravitational acceleration in the $i$ direction, $p$ is pressure, $\mu$ is the laminar viscosity, and the operator $\delta_{ij}$ is unity for $i=j$ and zero when $i\neq j$.

The equations for the conservation of a chemical species, $l$ and of energy may be expressed respectively as:

$$\frac{\partial}{\partial x_i}(\overline{\rho u_i}\,\overline{m_l})-\frac{\partial}{\partial x_i}\left(\overline{\Gamma_l\frac{\partial m_l}{\partial x_i}}-\overline{\rho u_j' m_l'}\right)-\bar{P}_l=0 \quad (2)$$

and

$$\frac{\partial}{\partial x_i}(\overline{\rho u_i}\,\bar{\tilde{h}})-\frac{\partial}{\partial x_i}\left(\overline{\Gamma_h\frac{\partial \tilde{h}}{\partial x_i}}\right)+\frac{\partial}{\partial x_i}\overline{\rho u_i'\tilde{h}'}-\bar{S}=0 \quad (3)$$

In (2) $m_l$ stands for the mass fraction of $l$, $\Gamma_l$ is the mass diffusion coefficient for this species, and $P_l$ is its chemical rate of production. In (3), $\tilde{h}$ represents stagnation enthalpy, $\Gamma_h$ is equal to the fluid thermal conductivity divided by its constant-pressure specific heat, and $\bar{S}$ is a source term defined by:

$$\bar{S}=\bar{Q}_{\text{rad}}+\text{small terms} \quad (4)$$

where $\bar{Q}_{\text{rad}}$ is the net volumetric heat gain due to thermal radiation.

In addition to (2)–(4) we must also, of course, include the equation of mass continuity

$$\frac{\partial}{\partial x_i}(\overline{\rho u_i})=0 \quad (5)$$

*Turbulence model*

The 'two-equation' model[3], in which equations for the kinetic energy of turbulence, $k$, and its dissipation rate, $\varepsilon$, are solved, is considered appropriate. The correlations in (1) are expressed, in analogy with laminar flow[4], as:

$$-\overline{\rho u_j' u_i'}=\mu_t\left(\frac{\partial \bar{u}_i}{\partial x_j}+\frac{\partial \bar{u}_j}{\partial x_i}-\frac{2}{3}\frac{\partial \bar{u}_k}{\partial x_k}\delta_{ij}\right) \quad (6)$$

where $\mu_t$ is a 'turbulent' viscosity that may be related to $k$ and $\varepsilon$ by dimensional arguments:

$$\mu_t=C_\mu\bar{\rho}k^2/\varepsilon \quad (7)$$

where $C_\mu$ is a constant of the model. The turbulent exchange coefficient $\Gamma_{\phi,t}$ for any variable $\phi$, may be expressed as:

$$\Gamma_{\phi,t}=\mu_t/\sigma_{\phi,t} \quad (8)$$

where $\sigma_{\phi,t}$ is a turbulent Prandtl number of order unity. Turbulent transport correlations involving $\phi'$ are determined from the Boussinesq approximation:

$$\overline{\rho u_i'\phi'}=\Gamma_{\phi,t}\,\overline{\partial\phi/\partial x_i} \quad (9)$$

The differential equations for $k$ and $\varepsilon$ that we solve are:

$$\frac{\partial}{\partial x_j}(\overline{\rho u_j}k)-\frac{\partial}{\partial x_j}\left(\Gamma_k\frac{\partial k}{\partial x_j}\right)-\mu_t\frac{\partial \bar{u}_i}{\partial x_j}\left(\frac{\partial \bar{u}_i}{\partial x_j}+\frac{\partial \bar{u}_j}{\partial x_i}\right)+C_D\rho\varepsilon=0 \quad (10)$$

and

$$\frac{\partial}{\partial x_j}(\overline{\rho u_j}\varepsilon)-\frac{\partial}{\partial x_j}\left(\Gamma_\varepsilon\frac{\partial \varepsilon}{\partial x_j}\right)-C_1\frac{\varepsilon}{k}\frac{\partial \bar{u}_i}{\partial x_j}\left(\frac{\partial \bar{u}_i}{\partial x_j}+\frac{\partial u_j}{\partial x_i}\right)+C_2\bar{\rho}\frac{\varepsilon^2}{k}=0 \quad (11)$$

where $C_1$ and $C_2$ are further constants and $\Gamma_k$ and $\Gamma_\varepsilon$ are determined via (8).

The model constants presently used are well established in many previous furnace applications[5,6].

*Combustion model*

The combustion model is based on the ideal of a single step and fast reaction between the gaseous fuel oxidant, assumed to combine in stoichiometric proportion. Equal effective turbulent mass diffusion coefficients for the fuel and oxidant and an instantaneous reaction are also assumed[7,8]. As a consequence of these assumptions the flame thermodynamic state becomes related to a single passive scalar:

$$\phi\equiv sm_{\text{fu}}-m_{\text{ox}} \quad (12)$$

where $s$ is the stoichiometric oxygen requirement by mass, and $m_{\text{fu}}$ and $m_{\text{ox}}$ are the fuel oxidant mass fractions.

The mixture fraction $f$ is related to this quantity by:

$$f\equiv(\phi-\phi_0)/(\phi_1-\phi_0) \quad (13)$$

where the subscripts 1 and 0 designate the fuel- and oxidant-bearing streams. We further assume that the chemical kinetic rate is fast with respect to the turbulent transport rate; that fuel and oxidant cannot co-exist, so $m_{\text{fu}}=0$ for $m_{\text{ox}}\geqslant 0$ and $m_{\text{ox}}=0$ for $m_{\text{fu}}\geqslant 0$, and the concentrations $m_{\text{fu}}$ and $m_{\text{ox}}$ are related linearly to $f$ through (12) and (13).

The transport equation for the mixture fraction is given by:

$$\frac{\partial}{\partial x_i}(\overline{\rho u_i}\bar{f})-\frac{\partial}{\partial x_i}\left(\Gamma_f\frac{\partial \bar{f}}{\partial x_i}\right)+\frac{\partial}{\partial x_i}\overline{\rho u_i' f'}=0 \quad (14)$$

The above modelling, it may be noted, presumes a stationary thin flame envelope. The fluctuating nature of the turbulent reaction is more usually accommodated[9] through a modelled equation for the variance of the mixture fraction fluctuations.

We adopt a statistical approach to describe the temporal nature of the mixture fraction fluctuations. The time-averaged value of any property $\phi$ solely dependent on $f$ can then be determined from:

$$\phi=\int_0^1\phi(f)P(f)\,\mathrm{d}f \quad (15)$$

In the present work we have assumed the 'clipped normal' probability density function[10] which is characterized by just two parameters, and the mean square of the fluctuations $g\equiv\overline{(f-\bar{f})^2}$. A modelled transport equation

has been derived[11] for $g$ which runs:

$$\frac{\partial}{\partial x_i}(\overline{\rho u_i g}) - \frac{\partial}{\partial x_i}\left(\Gamma_g \frac{\partial g}{\partial x_i}\right) - C_{g1}\mu_t\left(\frac{\partial f}{\partial x_i}\frac{\partial f}{\partial x_i}\right)\frac{C_{g2}}{k}\bar{\rho}\varepsilon g = 0 \quad (16)$$

where $C_{g1}$ and $C_{g2}$ are additional adjustable parameters.

A simple and economical model for oil-fired furnaces is used in which it is assumed that the oil spray evaporates instantaneously.

*Thermodynamics model*

The mixture specific enthalpy may be defined by:

$$h \equiv \int_0^T \sum_{\text{all } j} m_j C_{pj}(T)\,\mathrm{d}T + m_{\text{fu}} H \quad (17)$$

where $C_{pj}$ is the constant-pressure specific heat of a species $j$.

Density is determined from the equation of state,

$$\bar{\rho} = p\left(RT \sum_{\text{all } j} m_j / M_j\right)^{-1} \quad (18)$$

where $p$ is pressure, $R_o$ is the universal gas constant, and $M_j$ is the molecular weight of species $j$. Since the $m_j$'s, as well as $T$, are all functions of $f$, the time-averaged density for use in the mean flow equations is again determined from (15).

*Soot model*

The distinctive feature of oil-fired flames is their significant soot content. The proportion of the total carbon content of the fuel which converts to soot is too small to influence significantly the overall flame heat release distribution. Rather, soot is of concern because its presence greatly augments the radiation heat transfer and because it is a pollutant. Most reasonably operated and maintained modern burners ensure complete combustion of soot. So the primary function of the soot model will be good characterizing of the optical behaviour of the flame. The soot content of heavy oil flames is so great that those of industrial dimensions approach the black body limit. In consequence the accurate prediction of the local soot concentration is not a prerequisite for the good calculation of the radiation transfer. This is indeed fortunate since the mechanisms of soot formation are far from being established even in the simplest laboratory flames[12].

A simple global expression similar to that used by Khan and Greeves[13] is chosen to characterize soot production:

$$P_{s+} = C_f P_{\text{fu}} \phi^n \exp(-E/T_g) \quad (19)$$

$C_f$ is a function which ideally depends on an easily definable fuel property such as the C/H ratio. The authors have simply tuned it to flame data and have found that a value of about 0.01 is appropriate[14]. Although the work of Khan and Greeves[13] was performed in connection with diesel engines we find that their values of 3 and 40200 cal/mol for $n$ and $E$ are useful. Soot production is essentially zero for equivalence ratios, $\phi$, less than that corresponding to the incipient sooting limit[15] and for $\phi$ in excess of a value corresponding roughly to the upper flammability limit. Following Khan and Greeves the upper and lower limits have been set to 2 and 8 respectively.

In one sense the determination of the soot burning rate poses a much less demanding modelling problem since the particle sizes are so small that near-particle diffusion cannot possibly be controlling, rather the combustion rate will be controlled by, the rate of mixing of the particle-bearing vortices with adjacent oxygen bearing material. A straightforward method of estimating this rate has been proposed by Magnussen and Hjertager[16] who, following conventional turbulence concepts[17], presume that the mixing rate is proportional to the magnitude of the time mean soot concentrations, and the timescale of the large scale turbulence motion $\varepsilon/k$. Their expression for the soot consumption rate is:

$$P_{s-} = A\bar{m}_s(\varepsilon/k) \quad (20a)$$

where $A$ is a model constant assigned the value 4 based on numerical experimentation. This relation will not be satisfactory in regions where the reaction rate is limited by oxygen deficiency in which case Magnussen and Hjertager propose:

$$P_{s-} = A\left(\frac{\bar{m}_{\text{ox}}}{\bar{m}_s S_s + \bar{m}_{\text{fu}} S_{\text{fu}}}\right)\bar{m}_s\left(\frac{\varepsilon}{k}\right) \quad (20b)$$

where the $S_s$ and $S_{\text{fu}}$ are the soot and fuel stoichiometric ratios. The alternative giving the smallest reaction rate is to be used.

*Radiation model*

The 'discrete transfer' radiation prediction procedure of Lockwood and Shah[18] has been utilized in this study. This method combined ease of use, economy and flexibility of application. This last feature is of particular importance in the real world of geometrically intricate combustion chambers. The claimed advantages of the method have now survived the rigours of several industrial applications[16,19].

The 'discrete transfer' method is founded on a direct solution of the radiation transfer equation for a direction which runs:

$$\frac{\mathrm{d}I}{\mathrm{d}s} = (k_g + k_s)\left(\frac{E}{\pi} - I\right) \quad (21)$$

where $I$ is the radiation intensity in a $\Omega$ direction, $s$ is distance in that direction, $E \equiv \sigma T_g^4$ is the black body emissive power, and $k_g$ and $k_s$ are respectively the gas and soot absorption coefficients. The scattering terms do not appear, although they are easily accommodated, since the only particulate matter occurring in the present application is the soot particles which are much too small to scatter significantly. Many radiation methods are based on the solution of the much more complex integro-differential equation which results when (21) is rewritten for the whole solid angle $\Omega$. In the authors' opinion this is unsatisfactory since the numerical solution treatment of such an equation is necessarily very elaborate.

The authors prefer to solve the much simpler equation (21) within discretizations $\mathrm{d}\Omega$ of the whole solid angle $\Omega$ about selected directions $\Omega$. Assuming that $E$, $k_a$ and $k_s$ are constant over a finite distance increment $\delta s$, (21) may be integrated to yield the simple recurrence relation:

$$I_{n+1} = \frac{E}{\pi}\{1 - \exp[-(k_g + k_s)\delta s]\} + I_n \exp[-(k_g + k_s)\delta s] \quad (22)$$

where $n$ and $(n+1)$ are successive locations along $\Omega$ separated by the increment $\delta s$. The relation is applied along the chosen $\Omega$ from known conditions at point Q, say (either guessed or pertaining to those of the previous iteration), on one wall to the point of impingement, P say, of the direction on an opposite wall.

If the hemisphere above P is discretized into subangles $d\Omega_r$, within which the intensity is considered to be uniform, the energy flux arriving at P is:

$$q_{+,p}=\int_{\pi} I_p\Omega\, d\Omega=\sum_{\text{all } r} I_p,\ \Omega\ d\Omega_r \qquad (23)$$

The wall boundary condition is:

$$q_{-,p}=(1-\varepsilon_w)q_{+,p}+\varepsilon_w E_w \qquad (24)$$

where $q_{-,p}$ is the energy leaving the wall at P, $\varepsilon_w$ is the wall emissivity, and $E_w=\sigma T_w^4$ is the wall emissive power. The value of $I_{o,r}$ at point Q, the initial value required for the application of the recurrence relation (22), is $q_{-,p}/\pi$. The net radiation heat flux is of course:

$$q_p=q_{+,p}-q_{-,p} \qquad (25)$$

The net heat gain or loss within a small control volume of the flow procedure is:

$$S_R=(I_{n+1}-I_n)\Omega\, d\Omega\, dA \qquad (26)$$

where the locations $n$ and $(n+1)$ correspond to the 'entry' and 'exit' of a direction $\Omega$ into and from a control volume, and $A$ is the cell wall area projected normal to $\Omega$. The energy sources $S_R$ are appended to the energy balance equation solved for by the flow code.

The gas absorption coefficient $k_g$ is calculated from the 'two grey plus a clear gas' fit of Truelove[20]. Water vapour and carbon dioxide are the prime contributors to the gaseous radiation. The total gas emittance is expressed by:

$$\varepsilon_g=\sum_n a_{g,n}(T)[1-\exp(k_{g,n}(p_w+p_c)L] \qquad (27)$$

where the summation $n$ is over the three gases of the assumed mixture, the $k_{g,n}$ are presumed constant with the temperature dependence of the emittance being accommodated in the weighting coefficients $a_{g,n}$, $p_w$ and $p_c$ are the partial pressures of the water vapour and carbon dioxide and $L$ is the path length. The values of the $k_{g,n}$ and $a_{g,n}$ are tabulated in Reference 20. The value of $k_g$ required for these calculations is obtained from the pseudo grey approximation:

$$\varepsilon_g=1-\exp(-k_gL)$$

which has worked well in many furnace heat transfer computations.

## NUMERICAL SOLUTION PROCEDURE

### *Preliminary considerations*

Nearly all industrial furnaces are three-dimensional and exhibit the disparity of scales, in that most of the combustion takes place within a volume surrounding the burner which occupies only a small proportion of total furnace volume, but requires a disproportionately large proportion of the total computational grid. Furthermore, most burners generate axisymmetric (or very nearly so) flames in their immediate vicinity and in this region the flame is often relatively insensitive to the details of the flow elsewhere in the furnace. Therefore, the economy of the computations is very considerably enhanced by the separate calculation of the burner and bulk glass furnace combustion chamber regions.

In the present application, the burner region is calculated with an axisymmetric model. There are many models of that kind and they have been thoroughly tested[21,22]. The two-dimensional calculations yield a good resolution of the burner region and provide the inlet conditions for the three-dimensional calculations of the glass furnace combustion chamber. The matching between the two subcodes was effected along a frontier in the plane of the burner quarl exit. The choice of location for the frontier plane was dictated by the desire that convection there should everywhere have a strong axial component in the positive direction, that is towards the combustion exit. The frontier then becomes a 'parabolic' rather than an 'elliptic' interface. Since the linkage between the two subcodes at the frontier is one way rather than two way there was no need for interaction between them.

The question arises as to what are appropriate frontier boundary conditions for the burner region subcode. We have got round this difficulty by extending the burner region computations which, take advantage of the cyclic axial symmetry of burner, throughout the whole furnace length. The computational penalty of so doing is not very great and the inaccuracy due to the neglect of the three-dimensional effects of the combustion volume at the one way frontier must be small.

The important features of the matching procedure are the manner of ensuring continuity of mass, flux of energy etc. between the zones and the allowance made for the possibility (which we expect to be remote but do not wish to exclude) of two-way interactions between them. The former requirement is achieved by evaluating the total contact between the (small) control volumes of the burner zone and the (larger) volumes of the outer zone and then working out suitable average values of the densities, normal velocities and which, when all multiplied together give flux continuity.

In practice calculations are first performed for the burner zone, using the best available methods for estimating the boundary conditions. Then the main furnace zone is computed, using the predicted variables in the plane of the burner quarl exit from the burner calculation as boundary conditions. Although in tests we have then gone on to repeat this overall process using the outer zone results as the new burner boundary conditions, we have found the changes to be less than a few per cent, thereby confirming our supposition that, given a 'reasonable' estimate of the conditions at the burner boundary, iteration between zones is unnecessary, at least for the case we have studied.

### *Method of solution*

The finite difference method used to solve the equations entails subdividing the furnace into a number of finite volumes or 'cells'. *Figure 2a* shows a typical grid used for the axisymmetrical burner region, and *Figure 2c* the computational grid used for the three-dimensional furnace. Both solution algorithms are embodied in versions of TEACH program[23,24] for two- and three-

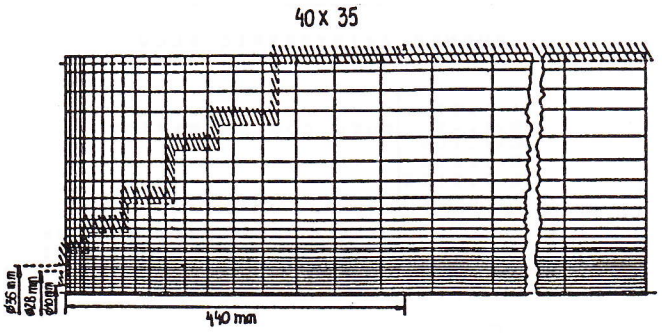


*Figure 2a* Computational grid. Two-dimensional burner region

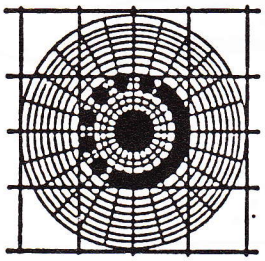

*Figure 2b* Computational grid. Plane of the burner quarl exit

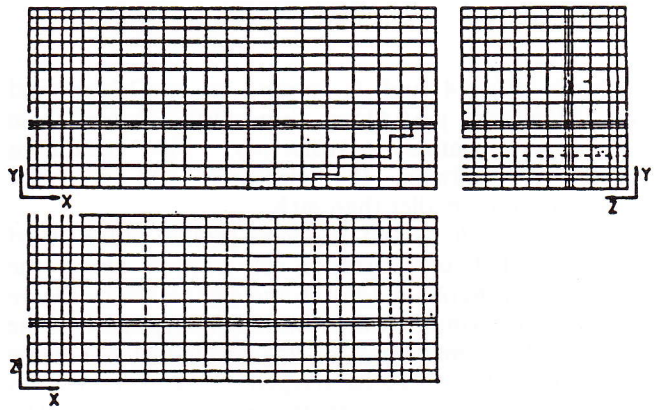


*Figure 2c* Computational grid. Three-dimensional furnace

dimensional recirculating flows. The convection terms were discretized by the hybrid central/upwind method[25]. The resultant difference equation has the form:

$$(a_p - S_p)\phi_p = \sum_n a_n \phi_n + S_0 \tag{28}$$

where $a_p \equiv \sum a_n$ and $\sum_n$ denotes summation over the six neighbouring nodes. One such equation exists for every scalar variable at every grid node. In the case of the velocities similar equations apply, but the control volumes are displaced such that they pass through the pressures driving the component in question, necessitating minor changes to the coefficient expressions.

The velocities and pressures are calculated by a variant of the SIMPLE algorithm[26]. As presented there, this algorithm involves the solution of the momentum equations using the prevailing pressures $\bar{p}^*$ to yield an intermediate velocity field denoted by $\bar{u}^*$; then velocity corrections are defined, linked to corresponding pressure corrections by relations of the form:

$$\bar{u}'_{j.b} = D^u_n(\bar{p}'_n - \bar{p}'_p) \tag{29}$$

where $D^u_n \equiv \partial u_{j.b}/\partial(p_n - p_p)$ is evaluated from the relevant momentum equation. Equation (29) is substituted into the integrated form of the continuity equation to give:

$$a_p \bar{p}' = \sum_n a_n \bar{p}' + S_0 \tag{30}$$

from which $p'$, and hence $u'$, is determined. Equation (30) may be recognized as a form of Poisson's equation for the pressure correction, in which $S_0 \equiv -\sum_b \dot{m}_b$ is the local continuity imbalance of the momentum-based $\bar{u}^*_j$ velocities. Following solution of this equation, the corrections are applied by setting $\bar{u}_j = \bar{u}^*_j + \bar{u}'_j$, $\bar{p} = \bar{p}^*_j + \bar{p}'_j$, and the entire procedure is repeated until momentum and continuity are both satisfied.

The calculations of the remaining dependent variables, as well as the updating of the thermodynamic and transport properties, are imbedded into the above sequence, but are not necessarily invoked at every cycle. For example, the radiation variables are recalculated less frequently than the others.

The solution of the individual equation sets is obtained by a form of Gauss–Seidel line-by-line iteration.

## RESULTS AND DISCUSSION

### *Some computational information*

The present prediction procedure has been applied for the solution of the process in a full scale industrial glass furnace with the real operating conditions. The total mass flow of fuel and oxygen were 0.03 and 0.105 kg/sec respectively. This represents 2% excess of oxygen. The fuel is injected at 393 K and the oxygen at 300 K. The fuel composition is 86% of carbon and 14% of hydrogen. The inlet axial velocities of fuel and oxygen were 127.5 and 200 m/sec. The radial and tangential velocities were set to zero due to the swirl absence. The kinetic energy of turbulence at the inlet is assumed to be 0.06% of the kinetic energy of the mean flow and its dissipation rate, $\varepsilon$, is calculated from the relation:

$$\varepsilon_{\text{inlet}} = 6.0 k^{1.5}_{\text{inlet}}/l$$

where $l$ is a characteristic length scale.

The furnace and the computational grids employed are sketched in *Figures* 1 and *2a*, *2b* and *2c*.

The burner quarl geometry is shown in *Figure 2a* together with the employed grid of $40 \times 35$ nodes in the axial and radial direction respectively.

At the outflow boundary of the two-dimensional burner region, all the dependent variables are governed by a zero axial gradient condition.

For the three-dimensional predictions a numerical grid comprising $NI \times NJ \times NK = 20 \times 13 \times 12$ grid nodes was used as represented in *Figure 2c*. The bottom wall (batch interface) is discretized and treated in a stepwise fashion. In the present case the small curvature of the roof was neglected.

The inlet conditions for the three-dimensional main combustion chamber were specified from spatial averaging of the results obtained from the axisymmetric calculations. *Figure 3* shows some of the predictions obtained with the axisymmetric model. *Figure 3a* shows the velocity field in the near region of the burner and *Figure 3b* shows the fuel concentration field. At the solid-wall boundaries of the furnace the temperature is equated to the measured values that were of 1723 K at the top and side walls and 1623 K at the bottom wall of the furnace.

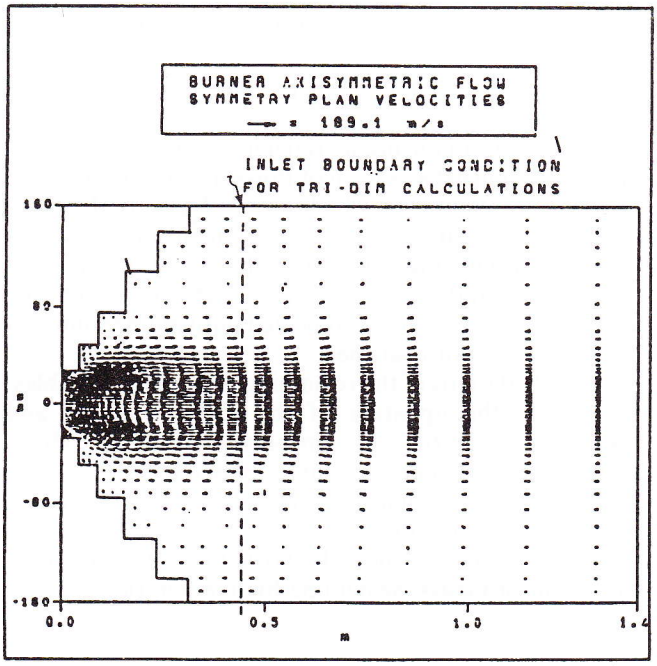


*Figure 3a* Predicted velocity in the near region of the burner

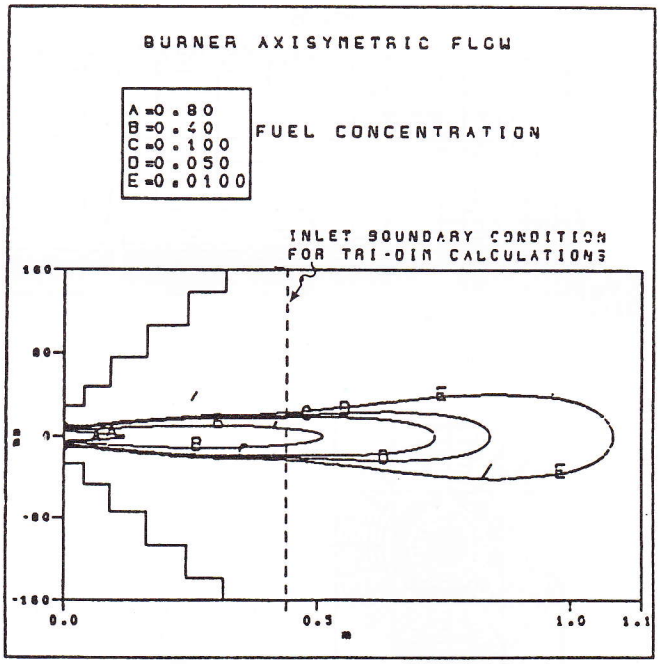


*Figure 3b* Predicted fuel concentration field in the near region of the burner

At the outflow boundary, all the dependent variables except the $w$ velocity component are governed by a zero-gradient condition. The $w$-velocity component at the outflow boundary is determined so as to satisfy the mass conservation principle for the calculation domain as a whole.

Convergence was achieved when the normalized residuals for the three momentum equations and mass conservation were less than $5 \times 10^{-3}$. This was achieved after 1457 iterations, that corresponds to 31 CPU hours in a MicroVAX II.

*Validation of the model*

One of the main purposes of the present study was to validate the predictions of the model against experimental data acquired in the large furnace described above.

The experimental data of temperature and oxygen were made along traverse paths in horizontal planes located at several distances above the bottom wall of the furnace[27].

*Figure 4a* shows the measured and predicted gas temperature in a transverse path located at $x=0.715$ m from the burner and $y=0.82$ m above the bottom floor (referred as hole no. 1). *Figure 4b* shows a similar comparison for the hole no. 2 ($x=1.205$ m and $y=0.707$ m).

The maximum temperature observed in *Figure 4b* (hole no. 2) is higher than the maximum temperature in *Figure 4a* (hole no. 1) as the hole no. 2 is below the burner centreline and in the direction of the mixing region of fuel and oxygen streams.

Owing to technological limitations it was not possible to cross the flame and measure after $z=0.7$ m[27]. Nevertheless the satisfactory agreement obtained for $z \leqslant 0.7$ m, suggests that the temperature is well predicted for the other half of the furnace.

The discrepancy between predictions and measurements observed is considered satisfactory for engineering purposes.

*Figure 4c* and *4d* shows measured and predicted temperature profiles corresponding to the transverse path through holes 4 and 6, located at $x=2.31$ m and $x=2.71$ m and $y=0.615$ m respectively. Again these results are entirely satisfactory. The maximum discrepancy between the measured and predicted temperature is smaller than 80 K.

*Figures 5a*, *5b*, *5c* and *5d* shows profiles of measured and predicted concentration of oxygen along the transverse paths of holes 1, 2, 3, and 4 respectively. *Figure 5a* shows an asymmetric distribution of oxygen across the plane with its maximum of 9% located at the flame centreline. The predicted oxygen concentration is in satisfactory agreement with the measured values. The results show that in a large region of the furnace the oxygen concentration is approximately 2%. This value corresponds to the oxygen concentration of the flue gases.

Hole 2 is located at a distance of 1.205 m in the direction of the flame tip. This explains the low measured and predicted values of oxygen concentrations shown in *Figure 5b* for $z=0.6$ m.

The predicted flame length (based on the definition of 'chemical length'—distance from the burner exit to the point of stoichiometric fuel concentration) was 1.63 m, which is in good agreement with the visual estimation of the flame length of $1.7 \pm 0.2$ m.

*Figures 5c* and *5d* shows that the values of the oxygen concentrations become more uniform as a result of the transport process of the 'excess' of oxygen into the burner centreline. The measured and predicted oxygen concentrations are in satisfactory agreement.

*Discussion*

Some general aspects of the models predictions are illustrated by *Figures 6–11*.

*Figure 6a* shows the predicted projections of the velocity vectors on three vertical planes: near the right side wall, near the centreline of the burner and near the left side wall. This Figure shows that the main jet flow goes across all the furnace length, impinges on the front wall and forms a large recirculation zone on the upper

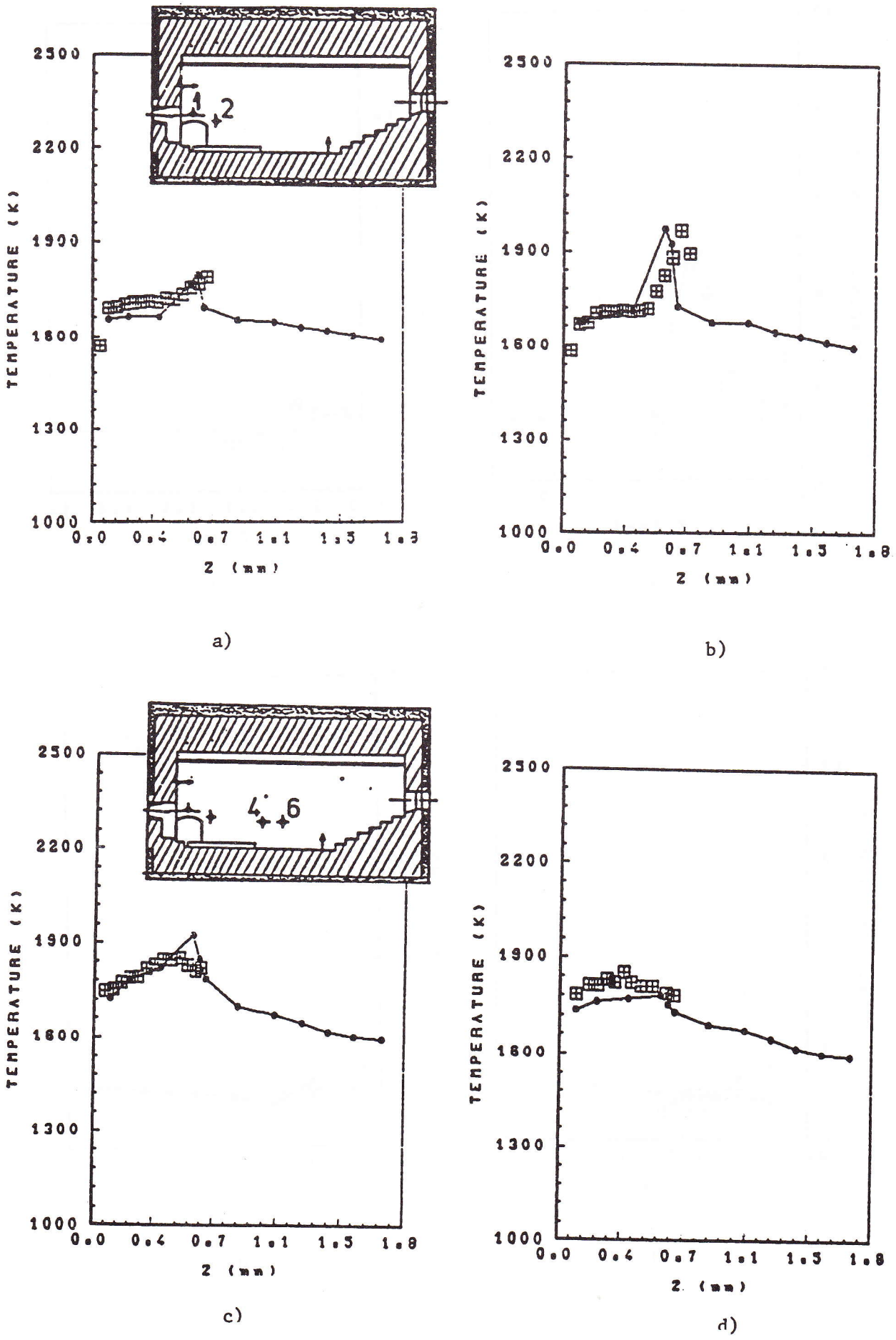


*Figure 4* Measured and predicted gas temperature. (a) Hole number: (a) 1; (b) 2; (c) 4; (d) 6. +, Measured values; ●, computed values

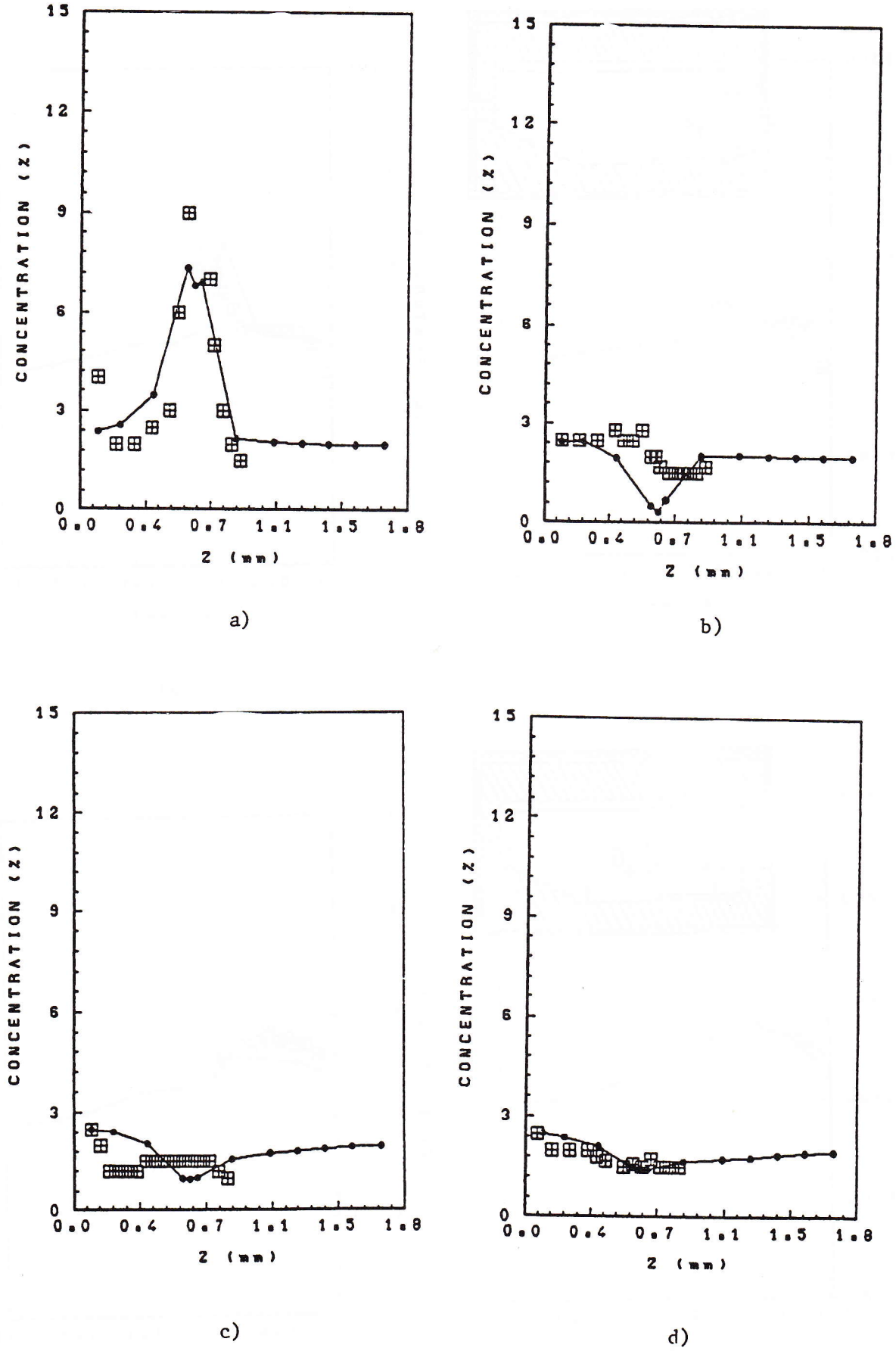


*Figure 5* Measured and predicted oxygen concentration profiles. Hole numbers: (a) 1; (b) 2; (c) 4; (d) 6. +, Measured values; ●, computed values

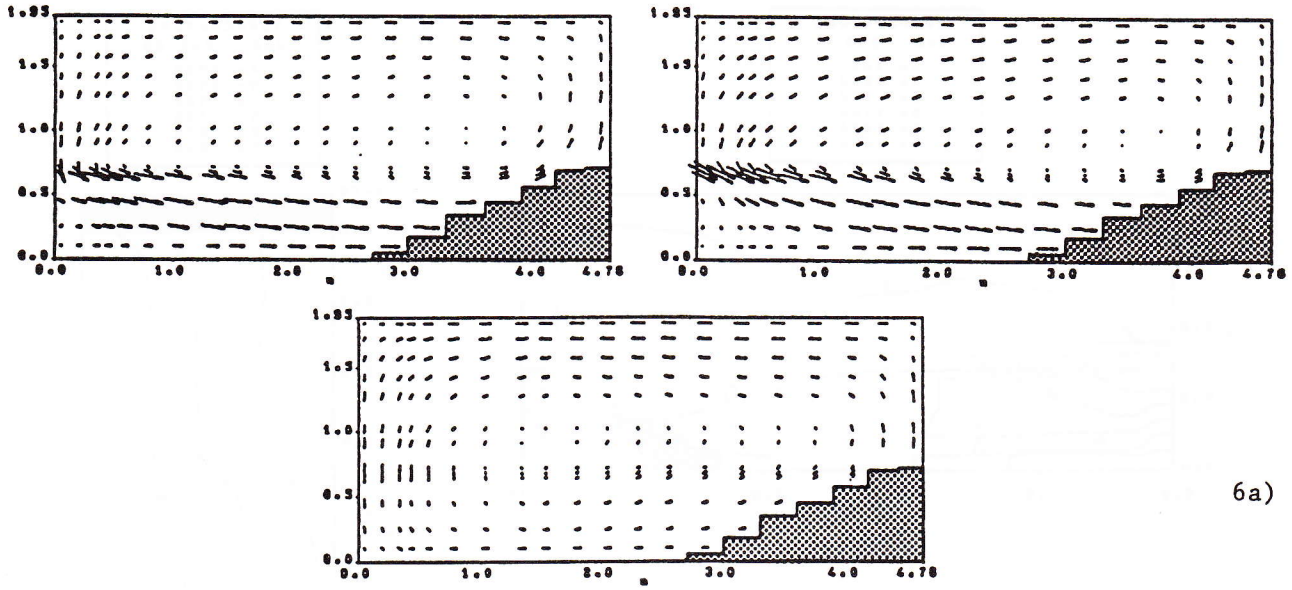

6a)

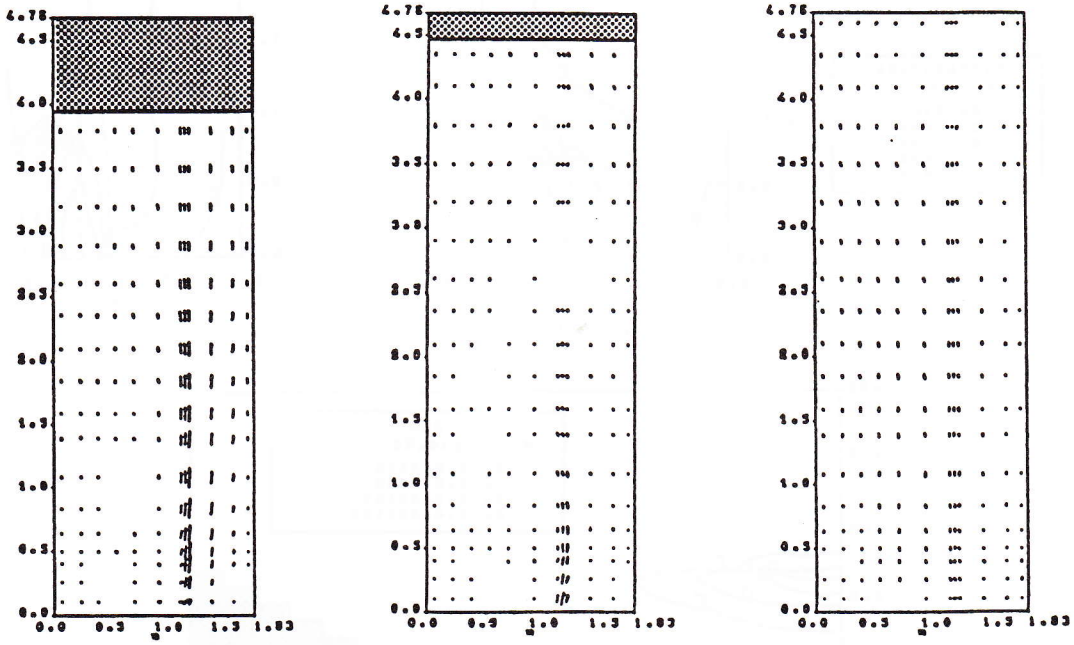

6b)

*Figure 6* Predicted velocity vectors. (*a*) *K*-plan velocityes=14.1 m/sec: $K=3$, $z=0.41$ m; $K=6$, $z=0.60$ m; $K=10$, $z=1.38$ m. (b) *J*-plan velocities=18.8 m/sec: $J=3$, $y=0.43$ m; $J=6$, $y=0.73$ m; $J=10$, $y=1.43$ m

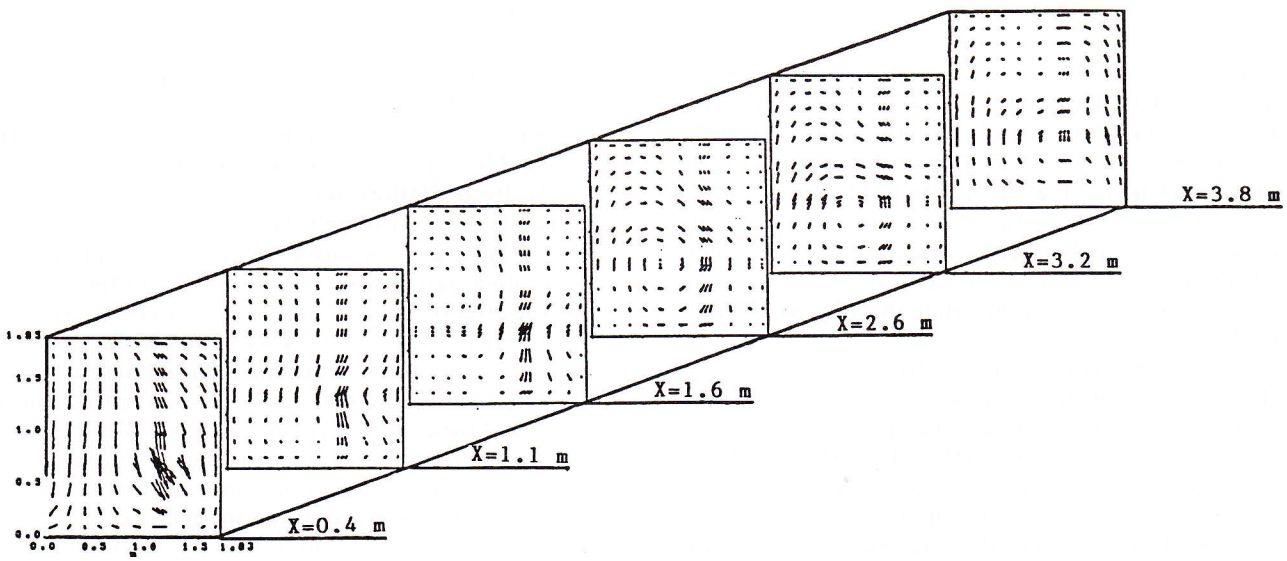


*Figure 7* Predicted velocity vectors for $x=$cte planes; =8.6 m/sec

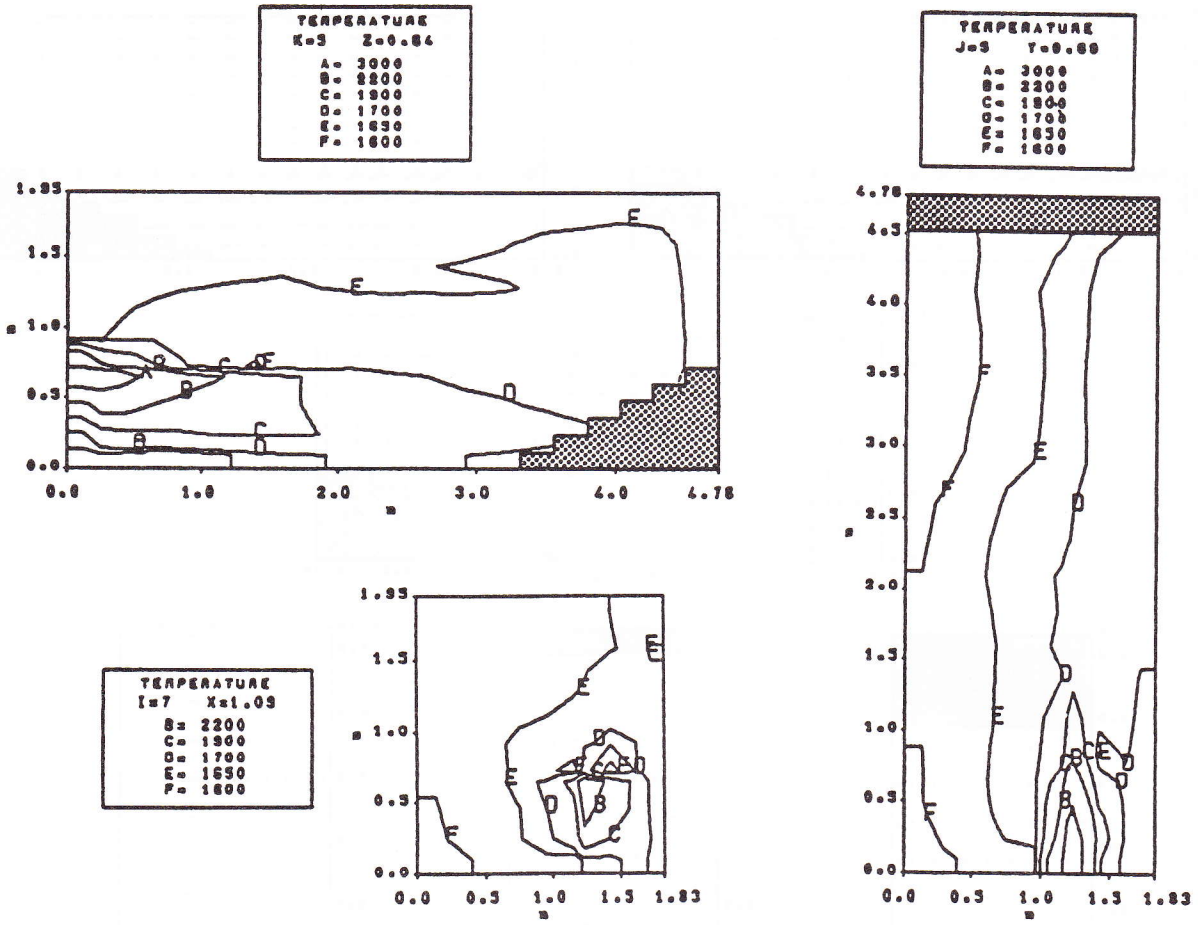


*Figure 8* Predicted gas temperature field

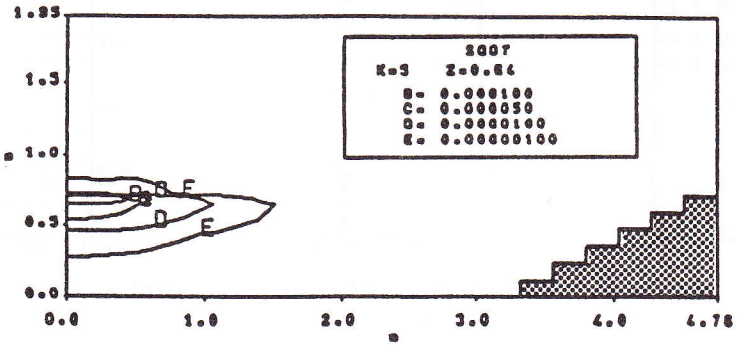


*Figure 9* Predicted soot concentration

portion of the furnace. *Figure 6b* shows the predicted projections of the velocity vectors on three horizontal planes: near the bottom wall, near the centreline of the burner and near the roof. This Figure shows that, close to the roof, the main flow is inverted. The flow will be orientated to the outlet with a strong downwards velocity component, as can be seen in *Figure 7*, for the plane parallel to the front wall at a distance of $x = 0.4$ m of this wall. This Figure also shows that the flow is strongly three-dimensional.

*Figure 8* shows temperature contours predicted by the model is selected in three planes: $z$, $x$, and $y$ constant. This Figure shows that in the reaction zone the temperature is higher than 3000 K. The adiabatic flame temperature for these conditions is about 8000 K. This difference is due to the strong radiation effects present in this large furnace. Outside the flame region the temperature distribution is near homogeneous.

The predicted contours of soot concentration are shown in *Figure 9*. The maximum soot mass concentration ($5 \times 10^{-4}$ kg/m$^3$) occurs near the burner region. Thereafter soot mass concentration decreases rapidly by oxidation and at the $x = 1.7$ m plane it is practically zero. Although there are no measured values of soot mass concentration in this particular furnace, these values agree with measurements in other furnaces (e.g. the experimental results reproduced by Abbas[28]). The soot mass concentration is zero at the outlet, a result that is very important due to the pollutant nature of soot.

A strong similarity was observed between the contours of $m_{soot}$ and the countours of $m_{fu}$. This confirms the strong influence of the amount of insufficiently mixed fuel in regions of high temperature in the soot formation phenomena as expressed in the model used.

*Figure 10* shows the contours of mass fraction of $O_2$ for three planes at $z$, $x$ and $y$ constant. The oxygen contours

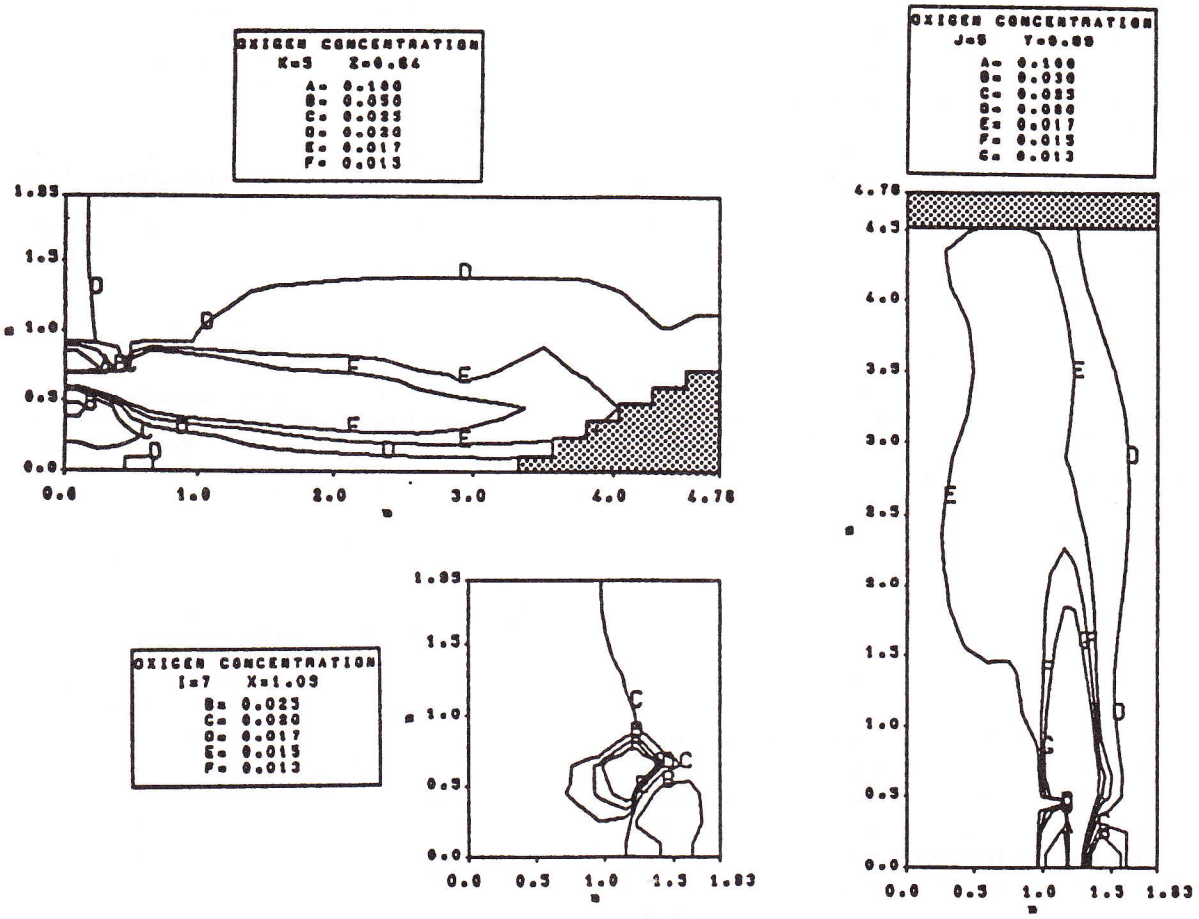


*Figure 10* Predicted contours of mass fraction of $O_2$

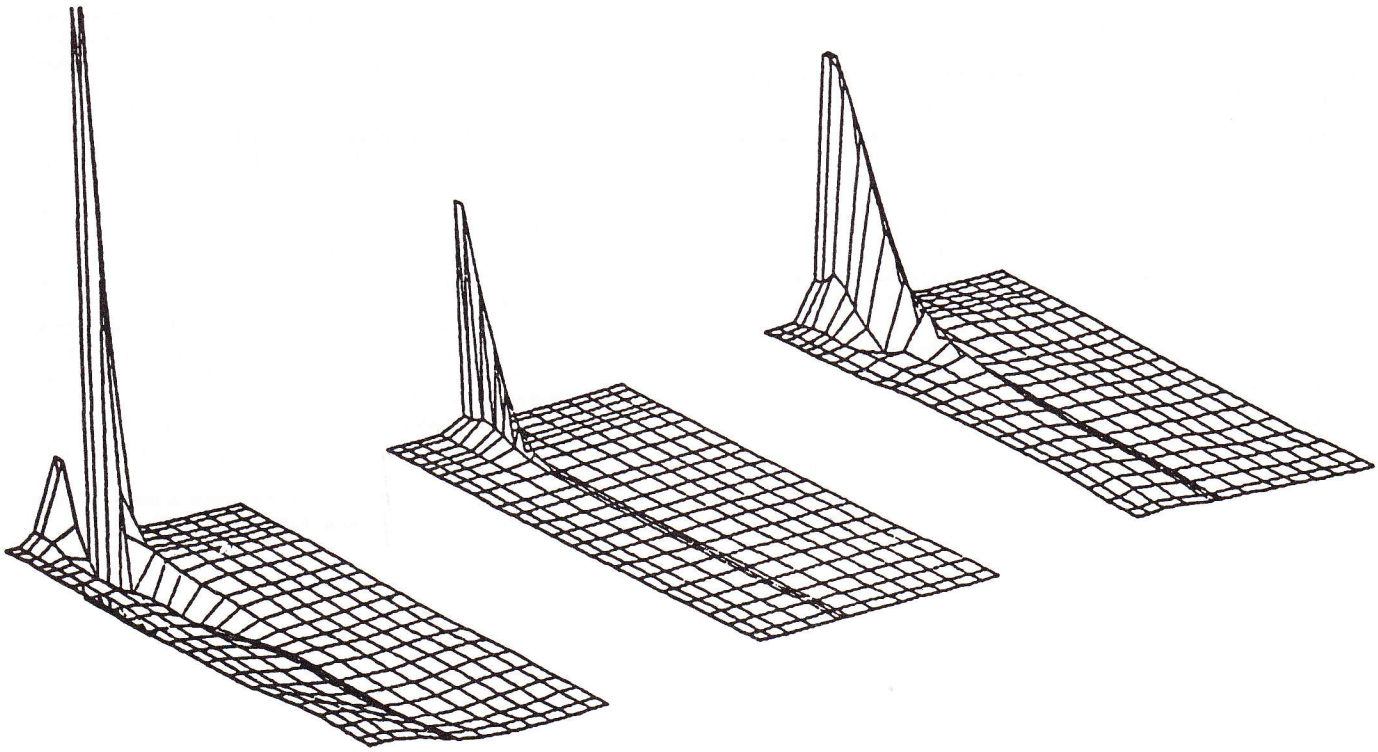

*Figure 11* Predicted concentration of $O_2$, fuel and temperature ($Y$=0.64 m)

reflect the flame location but because of the excess oxygen, the concentration of $O_2$ does not fall to zero.

*Figure 11* shows a three-dimensional plot of concentration of $O_2$, fuel and temperature for a plane parallel to the bottom wall, crossing the fuel injection. It can be seen that out of the flame region, the concentrations and temperatures are rather uniform, denoting the presence of a short flame and very important radiation effects.

## CONCLUSIONS

The predictive tool described herein should offer designers a good deal of encouragement. On the whole, the prediction procedure described stands up well to the validation test. The paper has described the application of a very useful and general prediction procedure to a real-life industrial furnace.

In the numerical treatment of this furnace some sources of inaccuracy may be present. The application of the hybrid/central upwind together with a numerical grid of $20 \times 13 \times 12$ may lead to numerical diffusion. Other errors are present due to the stepwise treatment of some of the furnace walls. These sources of error together with the simplicity of the turbulence and combustion model proved to be, in the present furnace (operating with oxy-fuel conditions) minor. This is a consequence of the importance of the radiation. The radiation model employed in this study proved to be very efficient; however, owing to the temperature field variation form 8000 K in the first iterations to 1800 K in the convergent solution, strong under-relaxation (0.1) was employed. Therefore the convergence was achieved after 1457 iterations.

We can conclude that oxy-fuel combustion in real furnaces can be predicted accurately, for engineering purposes, with the standard modelling if an efficient radiation model is employed.

## ACKNOWLEDGEMENT

The authors wish to acknowledge Metal Portuguesa for technical advice and the Commission of the European Communities (DG XII) for financial support of this work.

## REFERENCES

1 Gosman, A. D., Lockwood, F. C., Megahed, I. E. A. and Shah, N. G. The prediction of the flow, reaction and heat transfer in the combustion chamber of glass furnace, *AIAA 18th Aerospace Sci. Mtg, California* (1980)

2 Carvalho, M. G. and Loclwood, F. C. Mathematical simulation of an end-port regenerative glass furnace, *Proc. Instn Mech. Engrs*, **199**, 113 (1985)

3 Launder, B. E. and Spalding, D. B. *Mathematical Models of Turbulence*, Academic Press, New York (1972)

4 Hintze, J. O. *Turbulence*, McGraw-Hill, New York (1959)

5 Meghed, I. E. A. The prediction of three-dimensional gas-fired combustion chamber flows, *PhD Thesis*, London University (1979)

6 Carvalho, M. G. Computer simulation of a glass furnace, *PhD Thesis*, London University (1983)

7 Pun, W. M. and Spalding, D. B. A procedure for predicting the velocity and temperature distributions in a confined steady, turbulent, gaseous diffusion flame, *Proc. Int. Astronaut. Fed. Mtg, Belgrade* (1967)

8 Bilger, R. W. 'Turbulent flows with nonpremixed reactants, turbulent reacting flows, *Topics in Applied Physics* (Ed. P. A. Libby and F. A. Williams), Springer-Verlag, Berlin (1980)

9 Carvalho, M. G. and Lockwood, F. C. Prediction of a glass furnace, *Technical Note*, Mech. Eng. Dept, Imperial College (1981)

10 Lockwood, F. C. and Naguib, A. S. The prediction of the fluctuations in the properties of free, round jet, turbulent diffusion flames, *Combust. Flame*, **24**, 109 (1975)

11 Spalding, D. B. Concentration fluctuations in a round, turbulent free-jet, *Chem. Eng. Sci.*, **26**, 96 (1971)

12 Wagner, H. G. G. Soot formation in combustion, *Proc. 17th Int. Combustion Symp.*, Combustion Institute, Pittsburgh (1978)

13 Khan, I. M. and Greeves, G. A method for calculating the formation and combustion of soot in diesel engines; *Heat Transfer in Flames* (Ed. Afgan and Beer), pp. 391–402 (1974)

14 Abbas, A. S., Koussa, S. S. and Lockwood, F. C. The prediction of a variety of heavy oil flames, *Proc. ASME Winter A. Mtg, Washington* (Special Session on Two Phase Combustion Liquid Fuels) (Nov. 1981)

15 Glassman, I. and Yaccarino, P. The temperature effect in sooting diffusion flames. *Proc. 18th Int. Combustion Symp.*, Combustion Institute, Pittsburgh (1981)

16 Magnussen, B. F. and Hjertager, B. H. On mathematical modelling of turbulent combustion with special emphasis on soot formation and combustion, *Proc. 16th Int Combustion Symp.*, Combustion Institute, Pittsburgh (1976)

17 Tennekes, H. and Lumley, J. L. *A First Course in Turbulence*, MIT Press, Cambridge (1973)

18 Lockwood, F. C. and Shah, N. G. A new radiation solution method for incorporation in general combustion prediction procedures, *Proc. 18th Int. Combustion Symp.*,Combustion Institute, Pittsburgh (1980)

19 Carvalho, M. G., Durao, D. F. G. and Lockwood, F. C. Computation of thermal radiation for gas turbine conditions, *65th AGARD/PEP Symp. Bergen* (1985)

20 Truelove, J. S. A mixed grey gas model for flame radiation, *AERE Harwell Report No. HL 76/3448/KE* (1976)

21 Gosman, A. D., Lockwood, F. C. and Salloja, A. P. The prediction of cylindrical furnaces gaseous fired with premixed and diffusion flames, *Proc. 17th Int. Combustion Symp.*, Combustion Institute, Pittsburgh (1978)

22 Durst, F., Pereira, J. C. F. and Wennerberg, D. A computer code for the calculation of axisymmetrical steady turbulent reactive flows with or without swirl, *LSTM*, University of Erlangen-Nurnberg (1982)

23 Gosman, A. D. and Pun, W. M. Calculation of recirculating flows, *Lecture Notes*, Dept Mech. Eng., Imperial College (1974)

24 Gosman, A. D., Humphrey, J. A. C. and Vlachos, N. S. TEACH-3E: a general computer program for three-dimensional recirculating flows, *Report CHT/76/10*, Dept Mech. Eng., Imperial College (1976)

25 Spalding, D. B. A novel finite difference formulation for differential expressions involving both first and second derivatives, *Int. J. Num. Meth. Eng.*, **4**, 551 (1972)

26 Caretto, L. S., Gosman, A. D., Patankar, S. V. and Spalding, D. B. Two calculation procedures for steady, three-dimensional flows with recirculation, *Proc. 3rd Int. Conf. Num. Meth. Fluid Dynam.*, Springer-Verlag, New York, p. 60 (1972)

27 Durao, D. F. G., Heitor, M. V. and Moreira, A. L. Temperature and species characteristics of the flow in a glass smelting kiln, *Report*, Instituto Superior Tecnico, Lisbon (1986)

28 Abbas, A. S. The prediction of the performance of heavy oil-fired combustors, *PhD Thesis*, London University (1982)